SSCL-Preprint-533

Cold Beam Tube Photodesorption and Related Experiments for the SSCL 20 TeV Proton Collider

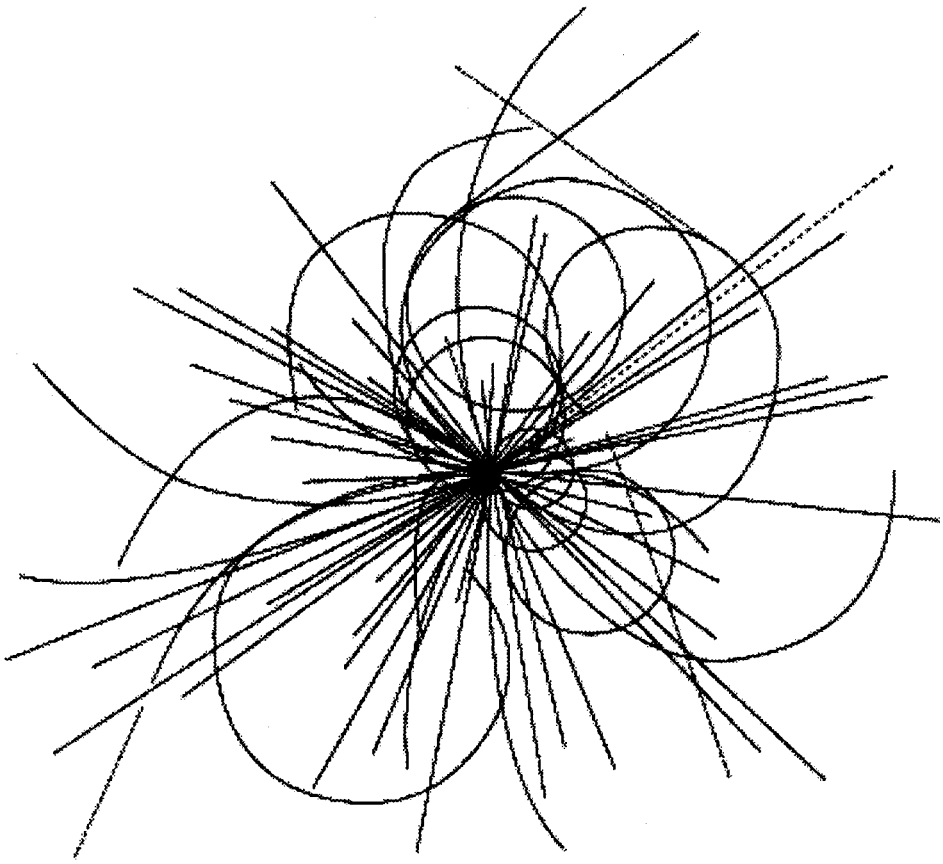

SSCL-Preprint-533
March 1994
Distribution Category: 414

V. Anashin
G. Derevyankin
V. Dudnikov
O. Malyshev
V. Osipov
C. Foerster
F. Jacobsen
M. Ruckman
M. Strongin
R. Kersevan
I. Maslennikov
W. Turner
W. Lanford

Superconducting Super Collider Laboratory

March 22, 1994

To the Preprint Librarian:

An author's name was inadvertently left off the front cover. Please replace the November 1993 version of this report (SSCL-Preprint-533). Your help in this matter is greatly appreciated.

SSCL-Preprint-533

Cold Beam Tube Photodesorption and Related Experiments for the SSCL 20 TeV Proton Collider*

V. Anashin, G. Derevyankin, V. Dudnikov, O. Malyshev, and V. Osipov

Budker Institute of Nuclear Physics
Novosibirsk, Russia

C. Foerster, F. Jacobsen, M. Ruckman, and M. Strongin

Brookhaven National Laboratory
Upton, NY 11973

R. Kersevan, I. Maslennikov, and W. Turner

Superconducting Super Collider Laboratory†
2550 Beckleymeade Ave.
Dallas, TX 75237

W. Lanford

State University of New York–Albany
Albany, NY 12222

November 1993

*To be submitted to the *Journal of Vacuum Science & Technology.*
†Operated by the Universities Research Association, Inc., for the U.S. Department of Energy under Contract No. DE-AC35-89ER40486.

COLD BEAM TUBE PHOTODESORPTION AND RELATED EXPERIMENTS for the SSCL 20 TeV PROTON COLLIDER

V.V. Anashin, G. Derevyankin, V.G. Dudnikov, O.B. Malyshev, V.N. Osipov
Budker Institute of Nuclear Physics, Novosibirsk, Russia

C.L. Foerster, F.M. Jacobsen, M.W. Ruckman, M. Strongin
Brookhaven National Laboratory, Upton, NY 11973

R. Kersevan, I.L. Maslennikov, W.C. Turner
Superconducting Super Collider Laboratory, Dallas, TX 75237

W.A. Lanford
State University of New York-Albany, Albany, NY 12222

Abstract

The next generation of proton colliders that has been contemplated – the Superconducting Super Collider (SSC)[1] in the United States and the Large Hadron Collider (LHC)[2] at CERN – will be the first to encounter significant intensities of synchrotron radiation within the cold bore tube of superconducting magnets. Aside from removal of the synchrotron radiation heat load, the main problem encountered is how to deal with the magnitudes of photodesorbed gases. Choosing the beam tube to coincide with the cryosorbing magnet bore tube has the advantages of simplicity and, in principle, of providing very high pumping speed. Tightly bound molecules in the near surface layer (~100 Å) are converted by photodesorption to a steadily increasing surface density of physisorbed molecules. However, the effective pumping by the bore tube is greatly

reduced by the photodesorption of relatively weakly bound physisorbed molecules. In addition, the saturation vapor density of H_2 at the ~4.2 K temperature of the SSC cryostats exceeds, by a factor of fifty, the upper bound allowed by the nuclear scattering deposition of energy in the magnet cryostats. Consequently, accumulation of a monolayer of physisorbed H_2 must be avoided even locally. An alternative approach is to install a coaxial perforated tube or liner inside the magnet bore tube which allows the photodesorbed gases to be pumped out of the view of the synchrotron radiation photons. The purpose of the work described in this paper is to develop a methodology that will allow prediction of SSC beam tube vacuum – for simple, 4.2 K beam tubes and for distributed pump or liner configurations – and to provide the technical data required for choosing among the alternative possibilities. The first photodesorption experiments have been completed on the VEPP2M storage ring at the Budker Institute of Nuclear Physics (BINP). Additional photodesorption experiments are underway at BINP and are being planned for a beamline at the UV ring of the Brookhaven National Laboratory National Synchrotron Light Source (BNL NSLS). Related experiments at BNL measuring molecular sticking coefficients and at the State University of New York – Albany (SUNY-Albany) measuring the depth profile of hydrogen on beam tube surfaces are also beginning to yield data. New ideas for directly measuring molecular density inside a cryosorbing beam tube are under development - neutralization of H^- and H^+ beams at BINP and positron annihilation at BNL. A status report of these activities is given in the paper.

1.0 Introduction to Vacuum Issues in a Superconducting Proton Collider

The basic beam tube vacuum issues in the next generation of superconducting proton colliders are indicated in simplified form in Fig. 1. Circulating protons radiate photons as their orbits are bent by the superconducting dipole magnets. In the SSC (20 TeV, 72 mA, ρ = 10.1 km) the synchrotron radiation critical energy is 284 eV, the intensity is 1×10^{16} photons/m/s and the radiated power is 140 mW/m or 9 kW/ring. The SSC photons travel approximately 20 m before striking the beam tube at ~2 mrad angle of incidence. Some fraction of the photons desorb gas molecules (H_2, CH_4, CO and CO_2) which are then physisorbed to the beam tube wall (Fig. 1(a)). Desorption by scattered photons is significant so one has to contend with photodesorption from the entire circumference of the beam tube although the FWHM of the point of initial photon impact is ~2 mm. The physisorbed molecules are weakly bound to the beam tube surface (~20 meV for H_2) and themselves become an important source of photodesorption that builds up with time. We distinguish the desorption of tightly bound molecules from those that are physisorbed, and sometimes refer to desorption of tightly bound molecules as primary desorption and of physisorbed molecules as recycling. The term "tightly bound" includes chemical binding and any other form of binding that is not readily desorbed by warming the tube to room temperature or less. The molecular density inside a cryosorbing beam tube then has three components: (1) the photodesorbed tightly bound molecules, (2) the photodesorbed physisorbed molecules and (3) the thermally desorbed isotherm density of physisorbed molecules. For gases other than H_2 (and He if there are leaks) the isotherm density is negligible. The potential problems of the simple beam tube – photodesorption of physisorbed molecules and the H_2 isotherm density – are alleviated by the liner concept in Fig. 1(b). The liner is a coaxial perforated tube fitting inside the magnet bore tube. Physisorbed molecules accumulate behind the liner and out of the view of the photons. The effective surface area of the magnet bore tube can be increased many times by the addition

of cryosorbing material behind the liner, thus postponing increase of the H_2 isotherm density.

For comparison, synchrotron radiation in the Tevatron at FNAL (1 TeV, 5 mA, ρ = 0.76 km), the first superconducting proton collider, has critical energy 0.5 eV, intensity 4.5×10^{14} photons/m/s and radiated power 0.01 mW/m. Until now synchrotron radiation in proton colliders has had negligible vacuum and refrigeration consequences.

The vacuum requirements for a superconducting proton collider are made quantitative by considering the effect of beam gas interactions on: (1) the loss of luminosity and (2) the scattered beam power deposited in the cold mass of the cryostats. The first leads to a limit on the circumferentially averaged gas density. The second leads to a limit on local gas density. For the SSC, the goal for vacuum limited luminosity lifetime is 150 hrs. The vacuum limited luminosity lifetime $\tau_{L,vac}$ is given by a sum over species of circumferentially averaged gas densities $\bar{n}_j$;

$$\frac{1}{\tau_{L,vac}} = 2\sum_j \bar{n}_j \sigma_{pj} c \qquad (1)$$

where σ_{pj} is the total 20 TeV proton cross section on species j which leads to a proton lost from the beam (= 104 mb for H_2, 629 mb for CH_4, 958 mb for CO and 1500 mb for CO_2 at 20 TeV, including inelastic and elastic scattering) and c is the velocity of light. Although H_2 is generally the dominant gas desorbed one must pay attention to the others because of their larger cross sections. The 150 hrs luminosity lifetime then leads to upper bounds on average gas density; $3 \times 10^8/cm^3$ for H_2, $5.2 \times 10^7/cm^3$ for CO *etc.* The maximum power that can be deposited in the SSC magnet cryostats has been estimated to be ~0.6 W/m before the increase in temperature leads to a runaway increase in beam tube pressure and/or a magnet quench.[3] The locally scattered beam power per unit length P/L is given by a similar sum over local gas densities n_j;

$$P / L = I_b E_b \sum_j n_j \sigma_{pj} \qquad (2)$$

where E_b is the circulating beam energy = 20 TeV and I_b is the beam current = 72 mA. Since the most of the products from a single beam gas interaction are deposited over a downstream path length ~40 m we are imagining a local gas density bump extending over roughly this scale length or greater. If all of the scattered beam power winds up in the cryostat cold mass, which is not a bad approximation, then 0.6 W/m leads to local limits on gas density; 4×10^{10}/cm^3 for H_2, 7×10^9/cm^3 for CO *etc.*[4]

Since the saturated H_2 isotherm density at 4.2 K is ~2×10^{12}/cm^3, accumulation of a monolayer of H_2 must be avoided anywhere in the SSC and the time to accumulate a monolayer of H_2 sets an upper bound on the beam tube warm up interval. This problem could be avoided by decreasing the cryostat temperature, for example at 3 K the saturated H_2 isotherm density is ~3×10^8/cm^3. However this path was not chosen for the SSC. Since frequent beam tube warm ups are disruptive of normal operations we have set a design goal of one beam tube warm up per operational year (~2×10^{23} photons/m). For H_2 then the mean photodesorption coefficient should be in the range $\overline{\eta}(H_2) = 2 \times 10^{-5}$ molecules/photon for a beam tube ID = 40 mm and H_2 monolayer density $s_m = 3 \times 10^{15}$ / cm^2. If the liner approach is adopted then the cryosorber capacity should exceed the H_2 that is desorbed by ~2×10^{23} photons/m.

The temperature of a liner could be chosen to be at or near the temperature of the magnet bore tube or significantly higher, for example at a temperature where refrigeration capacity already exists – 20 K or 80 K at the SSC. Each choice has its advantages and disadvantages. Choosing the temperature to coincide with the magnet bore tube has the advantages of simplicity and elimination of the possibility of heat leaks to 4.2 K due to thermal shorts and thermal radiation from the liner. Choosing one of the higher temperatures has the advantages of improving the thermodynamic efficiency of removing the synchrotron radiation heat load and of decoupling the beam intensity from the 4.2 K

refrigeration capacity. However, in order to regulate the liner temperature, it would then be necessary to install high pressure gaseous He loops attached to the liner and inside the beam tube vacuum. This adds engineering complexity and risk of failure.

2.0 Outline of Cold Beam Tube Photodesorption and Related Experiments

In order to have a reasonable chance for success with the design of the SSC beam tube vacuum it is necessary to be able predict the evolution of gas density. Two years ago, when the work described in this paper was initiated, the basic data for doing this did not exist. Data from previous 4.2 K photodesorption experiments were limited to a maximum photon flux 1×10^{21} photons/m, or roughly one day of SSC operation, and extrapolation beyond this flux had large uncertainty.[5] Consequently the initial emphasis of our work has been to develop an experimental procedure for measuring beam tube photodesorption coefficients at 4.2 K for a given choice of material. This is a prerequisite for any optimization or selection of beam tube materials or indeed for choosing between a simple beam tube and a liner. This initial stage is nearing completion with measurement of 4.2 K photodesorption coefficients at BINP up to ~10^{22} photons/m, or ~ten days of SSC operation. Experiments with a simple beam tube and with a coaxial liner have allowed a clean separation of the photodesorption coefficients of tightly bound and physisorbed molecules. In the next round of experiments it is planned to extend the integrated photon flux to ~2×10^{23} photons/m, or one year of SSC operation. We have also planned to install a similar experimental apparatus at the BNL VUV ring to increase our measurement capability. So far the 4.2 K measurements have been restricted to the single beam tube material initially selected for the SSC – a particular type of electrodeposited Cu on a stainless steel tube. Others will be considered after the 2×10^{23} photons/m experiment has been completed with the original electrodeposited Cu. In parallel with the development of the 4.2 K apparatus we have been accumulating photodesorption data at room temperature for a variety of different beam tube materials as a pre-selection step for 4.2 K experiments.[6] This work has been done

primarily at the BNL NSLS UV ring. The beam tubes tested include two types of electrodeposited Cu, high purity bulk Cu, electroplated Cu with a Au layer and heat treated electrodeposited Cu. So far all the materials tested to an integrated photon flux of 10^{23} photons/m have desorption coefficients and integrated molecular yield within a factor of two of the originally tested electrodeposited Cu.

Nuclear reaction analysis (NRA) has been used to measure the surface concentration of hydrogen in the near surface layer of some of these materials to see if a correlation can be made with the amounts of photodesorbed H_2. These type of studies may eventually contribute to a better understanding of the origin of photodesorbed gas. Although photodesorption of technical beam tube materials has been studied for almost thirty years, mostly in the context of electron synchrotrons, there is not yet an understanding of the details of the photodesorption process; the chemical form of the molecules before they are photodesorbed, the relative contributions of the near surface layer and diffusion from the bulk material, the breaking of chemical bonds and recombination to form the molecules that eventually leave the surface *etc*. It is not necessary to have such an understanding in order to design a successful beam tube vacuum system. However, a deeper understanding could contribute to an optimized solution.

In order to fully characterize the beam tube vacuum it is useful to know the sticking coefficients and mean effective molecular speeds of the gas molecules that are present in addition to the photodesorption coefficients. Experiments using photoemission spectroscopy to measure the buildup of gas on a ~4.2 K surface at a controlled dosing rate have begun at the BNL VUV ring. So far clean evaporated Cu surfaces have been used. If these are successful giving quantitative measurements of sticking coefficients, the method will be extended to technical beam tube surfaces. Direct measurement of the velocities of photodesorbed molecules inside a ~4.2 K-beam tube are difficult. Direct measurement of the molecular density at 4.2 K, when combined with density measurements at room temperature and the assumption of thermal transpiration, are equivalent to measurements of

effective mean molecular speed. Two methods are being pursued to directly measure molecular density inside the 4.2 K beam tubes – measurement of the neutralization probabilities of H^- and H^+ beams at BINP and measurement of the positron annihilation rate at BNL. The first 4.2 K photodesorption experiment, completed in the SSC Central Design Group era, used a chopper to modulate the photon beam and a molecular beam type detector.[5] For that experiment measurement of the decay of H_2 density, when combined with an estimate of the sticking coefficient, can be used to estimate the mean H_2 velocity. It is possible that fast extraction of the VEPP2M electron beam and subsequent decay of the H^0 signal could be used in a similar way.

The remainder of this paper is organized into five sections: the basic equations useful for analyzing 4.2 K beam tube vacuum, experimental data, model vacuum calculations, new techniques for direct measurement of gas density in a 4.2 K beam tube and a summary and discussion of the direction of future work.

3.0 Basic equations for vacuum analysis of a cryosorbing beam tube exposed to synchrotron radiation

The following three equations are useful for describing the density of gas molecules in a cryosorbing beam tube exposed to synchrotron radiation;[7]

$$V\frac{\partial n}{\partial t} = \eta_1\dot{\Gamma} + \eta'\dot{\Gamma} - \sigma_w S_w * (n - n_e) - C * n + A_c D\frac{\partial^2 n}{\partial z^2} \tag{3}$$

$$A_w\frac{\partial s}{\partial t} = \eta_2\dot{\Gamma} + \sigma_w S_w * (n - n_e) - \eta'\dot{\Gamma} \tag{4}$$

$$x = \frac{\alpha y}{[(1-y)(1 + (\alpha - 1)y)]} . \tag{5}$$

In these equations, n is the molecular density, s is the surface density of physisorbed molecules, V(= πa^2) is the beam tube volume per unit axial length, A_w(= $2\pi a$) is the beam tube wall area per unit axial length, A_c(= πa^2) is the beam tube cross section area and $\dot{\Gamma}$ is the photon flux in photons/m/sec. Eqn. (3) describes the density n; the first term on the right is the desorption of tightly bound molecules with desorption coefficient η_1; the second term is the desorption of physisorbed molecules with desorption coefficient η'; the third term is wall pumping with sticking coefficient σ_w, ideal pumping speed $S_w = A_w\bar{v}/4$ and equilibrium isotherm density n_e; the fourth term is distributed pumping with pumping speed C per-unit axial length; the fifth term is axial diffusion with Knudsen diffusion coefficient $D = \frac{2}{3}a\bar{v}$. If the distributed pumping is by a liner we assume that the 4.2 K beam tube wall and cryosorber behind the liner have pumping speeds large compared to the liner conductance. Eqn. (4) describes the surface density of physisorbed molecules; the first term is due to direct conversion of tightly bound to physisorbed molecules by the incident photon flux, the second term is wall pumping and the third is photodesorption of physisorbed molecules. At low surface density the desorption of physisorbed molecules is expected to depend linearly on s; $\eta' = \eta_0'(s/s_m)$ where s is normalized to a monolayer density s_m. Eqn. (5) is a BET equation to describe the isotherm density; x(= s/s_m) is the normalized surface density, y(= n_e/n_{sat}) is the normalized volume density with saturation value n_{sat}, and α (= $e^{\theta/T}$) is a parameter.[8] Eqns. (3)–(5) may to applied to any gas species however at 4.2 K it is only necessary to retain the isotherm term for H_2.

Some of the solutions to Eqns. (3)–(5) have been discussed previously.[7] Here we are interested in the solutions for an infinitely long beam tube, which is a good approximation to the cold bore tube of a superconducting proton collider. For a simple 4.2 K beam tube with no distributed pumping the volume and surface densities are given by;

$$n = \frac{\eta_1\dot{\Gamma}}{\sigma_w S_w} + \frac{\eta'\dot{\Gamma}}{\sigma_w S_w} + n_e, \tag{6}$$

$$s = \frac{1}{A_w} \int_0^{\Gamma} (\eta_1 + \eta_2) d\Gamma \quad . \tag{7}$$

Since s is building up steadily with time n will also increase due to increasing η' and isotherm density n_e. If a liner is present with conductance C per-unit axial length then the surface density can reach a quasi steady state and the solution for density is given by;

$$n = \frac{(\eta_1 + \eta_2)\dot{\Gamma}}{C}. \tag{8}$$

The solution for the surface density is $s / s_m = \sigma_w S_w n / \eta_0' \dot{\Gamma}$ assuming $\eta_2 << \eta'$, which is a good assumption, and $n << n_e$. The remarkable thing about the liner solution is that it does not contain η' even though there is physisorbed gas on the liner; photodesorption of physisorbed gas is balanced by re-adsorption on the liner. Generally the density with a liner will decrease with time as the liner cleans up and the desorbed tightly bound gas is pumped outside the liner.

4.0 Experimental data

4.1 H2 isotherm and thermal desorption characteristic

The 4.2 K H_2 isotherm density for an electrodeposited Cu beam tube is shown in Fig. 2(a). The data were obtained with the same cryostat used for photodesorption experiments but with an additional small diameter perforated dosing tube inserted along the axis of the beam tube. For the data shown the H_2 dosing rate was 2.6×10^{12} $H_2/cm^2/sec$ and the duration of the entire experiment 2.9×10^3 sec. The same data were also obtained at dosing rates 2.6×10^{11} $H_2/cm^2/sec$ and 7.9×10^{11} $H_2/cm^2/sec$. The background density before dosing with H_2 was 3.6×10^8 H_2/cm^3. With dosing, the H_2 density increased to $9 \times 10^8/cm^3$ at adsorbed surface density 2.3×10^{15} H_2/cm^2 and then increased over three orders of magnitude to reach a saturation density $\sim 1.4 \times 10^{12}$ H_2/cm^3. The

isotherm vapor density reached 4×10^{10} H_2/cm^3, the local density limit allowable for the SSC design, at surface density $s_m = 3 \times 10^{15}$ H_2/cm^2, which we loosely refer to as the H_2 monolayer density for this particular beam tube material. The dosing tube was removed prior to photodesorption experiments.

In Fig. 2(b), we show thermal desorption data for H_2 and CO taken after a photodesorption experiment with an electrodeposited Cu beam tube. The pressure in Fig. 2(b) was measured at room temperature so the thermal transpiration correction needs to be applied to calculate pressure and density inside the cold beam tube. The H_2 desorption data, $T < 40$ K in Fig. 2(b), were taken with an ionization gage, the CO data, $T > 40$ K in Fig. 2(b), were taken with a capacitance gage. The H_2 is ~100% desorbed at $T = 20$ K.

4.2 Desorption coefficients at 4.2K

The experimental measurements of photodesorption coefficients in 4.2 K electrodeposited Cu beam tube (ID = 32 mm, length = 1 m) have been described in a recent report.[9] Here we summarize some of the results. The photodesorption coefficient η'/σ_w for 4.2 K physisorbed H_2 is shown versus H_2 surface density in Fig. 3. The data are reasonably well represented by a linear dependence; $\eta' = \eta_0'(s/s_m)$ with $\eta_0'/\sigma_w = 7.0 \pm 1.5$ and $s_m = 3 \times 10^{15}$ H_2/cm^2. The photodesorption coefficients for tightly bound H_2 and CO not previously desorbed are given in Fig. 4 up to photon flux 9×10^{21} photons/m. Data are shown for 4.2 K and 294 K experiments. All of the data in Figs. 3 and 4 have been taken with electrodeposited Cu. For a simple 4.2 K beam tube without a liner, we can estimate the photon flux Γ when the photodesorption of physisorbed H_2 molecules dominates photodesorption of tightly bound molecules; $\Gamma = s_m/\eta_0' = 4 \times 10^{18}$ to 4×10^{19} photons/m for $\sigma_w = 1.0$ to 0.1. For $\dot{\Gamma} \sim 10^{16}$ photons/m/sec, photodesorption of physisorbed H_2 will dominate H_2 gas density in a simple 4.2 K beam tube except for the first hour or less of photon exposure, independently of magnitude of η, until the H_2 surface density approaches one monolayer. The magnitude of η is important however since

it determines the rate of increase of the H_2 surface density, and therefore the magnitude of η' and the time to accumulate a monolayer of H_2. The photodesorption coefficients of tightly bound molecules in Fig. 4 show an overall trend of decreasing with increasing photon exposure and the room temperature coefficients are somewhat larger than 4.2 K coefficients. We estimate the total numbers of desorbed molecules by integrating the desorption coefficients over the measured range of integrated photon flux $\Gamma = 9 \times 10^{21}$ photons/m: for the 4.2 K data, 1.1×10^{19} H_2/m and 9.2×10^{17} CO/m; for the 294 K data, 4×10^{19} H_2/m and 6×10^{18} CO/m.

In Fig. 5 we have plotted the cumulative and differential photon fluxes required to desorb successive monolayers of H_2 (one monolayer = $A_w s_m = 3.1 \times 10^{18}$ H_2/m) for 4.2 K and 294 K; more data are shown for 294 K because that experiment was continued to 2×10^{23} photons/m. This information is crucial for deciding the issue of liner or no liner for the SSC Collider since it gives estimates of the frequency of interruption of operations due to beam tube warm ups (at design intensity, one day of operation = 8.6×10^{20} photons/m) as well as the number of warm ups required to reach the goal of less than one monolayer desorbed per-operational-year (2×10^{23} photons/m). If a liner approach were adopted the information is necessary to estimate required capacity of H_2 cryosorber. The 4.2 K data in Fig. 5 shows that the first monolayer is desorbed with the equivalent of 1.4 days integrated photon flux and by the fourth monolayer this has increased to 7 days. Simple extrapolation of the trend of the data indicates that between ten and twenty monolayers would be desorbed before reaching the level of one monolayer per-operational-year (2×10^{23} photons/m). Since this conditioning process would restart each time a section of the beam tube is replaced, this would seem to be an unacceptable burden on machine operation. Perhaps a better beam tube material or conditioning procedure can be found which reduces the desorbable H_2. Several suggestions have been made. We now have the experimental machinery in place to carry out comparative studies of such options. Of course this problem is avoided if a liner approach is used. This point was demonstrated

in the experiments measuring the desorption coefficients in Figs. 3 and 4; a liner was shown to effectively shield the cryosorbed molecules from the synchrotron radiation.

4.3 Sticking coefficients

Knowledge of the molecular sticking coefficients σ_w in Eqns. (3) and (4) is essential for understanding the dynamics of beam gas density. An apparatus has been assembled at BNL using photoelectron emission spectroscopy to measure sticking coefficients. Synchrotron light from a monochromator (photon energy = 170 eV) is beamed onto a surface and the intensity and energy spectrum of photoelectrons is measured with a hemispherical electrostatic energy analyzer and channeltron detector. The sample is attached to a continuous flow LHe cryostat and has temperature 4–5 K. Dosing gas is admitted to the vacuum chamber through a variable temperature nozzle which can be directed at the sample surface. It is planned to vary the temperature of the nozzle from 294 K to 40 K; the first measurements reported here are at 294 K. The surface that has been investigated so far is a clean evaporated 50–100 Å Cu film; once this is understood similar studies will be made with technical beam tube surfaces.

Figure 6a shows photoelectron energy spectra from the clean 4–5 K Cu surface and after a dose of seven Langmuirs of H_2 (one Langmuir = 1×10^{-6} Torr-sec = 1.45×10^{15} H_2/cm^2 at 294 K). The clean surface shows a sharp peak due to photoemission of Cu 3d electrons and a flat continuous inelastic electron spectrum from the Cu 3d peak to higher binding energies. The spectrum after exposure to 7 Langmuirs of H_2 shows an enhancement of the continuous spectrum below – 15 eV due to inelastic scattering on hydrogen. The data in Fig. 6(a) have been normalized to the same Cu 3d intensity. The absolute intensity of the Cu 3d peak actually decreases due to scattering on the adsorbed gas layer and it is this decrease in intensity that is used as a measure of the hydrogen surface density. An example of this is shown in Fig. 6(b); the electron energy analyzer has been tuned to the Cu 3d feature and the intensity plotted from 0 to 7 Langmuirs. A linear

decrease in intensity is observed between 0 and 2.3 Langmuirs; beyond 2.3 Langmuirs the intensity is flat indicating no further adsorption of H_2. We interpret this as the adsorption of one monolayer of H_2 and the flattening is due to the fact that the vacuum pressure is well below the saturation density of the H_2 isotherm. An estimate of the sticking coefficient is readily obtained from a simple flux balance; $\sigma_w \times 2.3 \times 1.45 \times 10^{15} = s_m$, or $\sigma_w = s_m/3.34 \times 10^{15} \sim 1$ for 294 K H_2 on a 4–5 K "clean" Cu surface. We don't actually know the monolayer H_2 density for the evaporated Cu surface used for this experiment, but if it is similar to what we have measured for an electrodeposited Cu beam tube then the sticking coefficient implied by the data in Fig. 6(b) is close to unity. However, the enhancement of the H_2 density over the substrate due to the formation of a gas jet by the doser has been neglected. In an identical experiment using CO (assumed to have unity sticking coefficient at 4 K), the enhancement factor was found to be about 10. This would reduce the estimated sticking coefficient for H_2 to approximately 0.1, a value in reasonable agreement with sticking coefficients derived from H_2 and D_2 molecular beam experiments on LHe cooled Cu(100).[10]

4.4 Depth profile of hydrogen in a metal surface

The 294 K H_2 photodesorption data in Fig. 5 indicate approximately 20 monolayers/m (1.8 Torr-l/m) of H_2 desorbed at 2×10^{23} photons/m. The source of this H_2 is a question of obvious interest. A first step in answering this question is to obtain the hydrogen depth profile of the surfaces we have studied. Such profiles have been obtained using nuclear reaction analysis (NRA) at the SUNY – Albany Accelerator Laboratory.[11] The particular reaction used is $^{15}N + H \rightarrow {}^{12}C + {}^{4}He + \gamma$ (4.43 MeV). This reaction has a narrow resonance (width $\Gamma = 1.8$ keV) at $E_{res} = 6.4$ MeV which is particularly effective for depth profiling surface H density. A sample is irradiated with a monoenergetic ^{15}N beam and the γ–ray intensity at 4.43 MeV measured with a barium germinate (BGO) scintillation detector. The depth profile is obtained by scanning the energy of the ^{15}N beam. The

samples irradiated have been cleaned with the standard cleaning procedure used for the photodesorption experiments. Fig. 7 shows the H depth profile results for the Silvex electrodeposited Cu used in the 4.2 K photodesorption experiments of Figs. 3–5 and, for comparison, for high purity Hitachi 10100 bulk Cu. Both samples show a sharp peaking of H density ~ 4×10^{22} H/cm^3 in a surface layer approximately 100 Å thick decreasing to a density ~1–2 $\times 10^{20}$ H/cm^3 in the bulk material. Compared to the bulk Cu atomic density 8.5×10^{22} Cu/cm^3 the fractional atomic percent of hydrogen is 0.1–0.2% below the surface layer. The surface densities obtained by integration are; 2.3×10^{16} H/cm^2 for the Silvex electrodeposited Cu and 2.6×10^{16} H/cm^2 for the Hitachi 10100 high purity Cu. Considering the very different manufacturing processes for these materials it is perhaps surprising how similar these results are, even in the bulk material far below the surface. It is likely that the thickness of surface layer observed is limited by the depth resolution of the profiling method and the actual surface layer is thinner and the peak H atoms/cm^3 is greater than given above. However the line integrated quantity H atoms/cm^2 is correct independently of the depth resolution.

We have previously obtained 294 K photodesorption data for both of the materials investigated in Fig. 7 up to an integrated photon flux $\Gamma = 10^{23}$ photons/m. It is interesting to compare the amount of photodesorbed hydrogen with the hydrogen surface densities measured with nuclear reaction analysis. This is done in Table I. The photodesorption experiments measure an amount of molecular hydrogen desorbed per meter length of beam tube. To convert this to an amount of H_2/cm^2, that can be compared with the NRA analysis, we have simply divided by the beam tube area per meter (=1005 cm^2/m), ignoring the question of the uniformity of photodesorption. Two things are notable in Table I: (1) the photodesorption and NRA data show closely similar results for Silvex electrodeposited Cu and Hitachi 10100 Cu and (2) the amount of hydrogen in the surface layer measured with NRA analysis is a significant fraction (~0.5) of the hydrogen photodesorbed by 10^{23} photons/m. The results reported here and photodesorption

experiments of a more extensive list of materials suggest that all the materials investigated have a similar hydrogen rich surface layer which is acquired during exposure to atmosphere and the cleaning process.

5.0 Model calculations

In this section we combine the equations given in Section 3 with the experimental data in Section 4 to predict beam tube vacuum conditions for the SSC. We first discuss the simple 4.2 K beam tube without a liner and then with a liner.

5.1 H_2 density in a 4.2 K beam tube

The H_2 density is the sum of the three terms given in Eqn. (6). The H_2 isotherm data in Fig. 2(a) is approximated by Eqn. (5) with $\alpha = 1.3 \times 10^4$, $s_m = 3 \times 10^{15}$ H_2/cm^3 and $n_{sat} = 2.0 \times 10^{12}$ H_2/cm^3. For the density due to desorption of tightly bound H_2 ($= \eta_1 \dot{\Gamma} / \sigma_w S_w$) there are two uncertainties: (1) we have measured the sum of η_1 and η_2 and not η_1 and η_2 separately and (2) we haven't measured the product of sticking coefficient and mean molecular speed $\sigma_w \bar{v}$ in the denominator. We will choose a typical value of desorption coefficient from Fig. 4 and divide it half into η_1 and half into η_2. For $\sigma_w \bar{v}$ we will take 2.1×10^4 cm/sec corresponding to the limiting cases $\sigma_w \sim 1.0, \bar{v} \sim 2 \times 10^4$ cm/sec and $\sigma_w \sim 0.1, \bar{v} \sim 2 \times 10^5$ cm/sec. As we will see below the H_2 density is either dominated by photodesorption of physisorbed gas or the H_2 isotherm and is insensitive to large uncertainty in the density due to photodesorption of tightly bound H_2. For the density due to desorption of physisorbed H_2 ($= \eta' \dot{\Gamma} / \sigma_w S_w$) we take η'/σ_w from Fig. 3 but we don't know $\bar{v}$ in the denominator. We will consider two cases bracketing what seems like the reasonable range of possibilities: $\bar{v} = 2.1 \times 10^4$ cm/sec and $\bar{v} = 1.8 \times 10^5$ cm/sec. The first is a lower bound corresponding to the beam tube temperature while the second is motivated by an analysis of the experiment of Bintinger *et al.*

Results of the calculations are shown in Fig. 8(a) for $\bar{v} = 2.1 \times 10^4$ cm / sec and Fig. 8(b) for $\bar{v} = 1.8 \times 10^5$ cm / sec where we have taken $\eta_1 = \eta_2 = 2 \times 10^{-4}$, corresponding to the magnitude of 4.2 K H_2 photodesorption coefficient at $\Gamma \sim 10^{22}$ photons/m. The three density components adding up to the total are labeled; (1) for photodesorption of tightly bound H_2, (2) for physisorbed H_2 and (3) for the H_2 isotherm. Until $\Gamma \sim 6 \times 10^{21}$ photons/m the density is dominated by desorption of physisorbed H_2 and after that by the rapid rise in the H_2 isotherm when the surface density of physisorbed H_2 has reached ~$3 \times 10^{15}/cm^2$. In neither case does the H_2 density rise above the local limit 4×10^{10} H_2/cm^3 until the isotherm density takes over. The transition to dominance by the isotherm depends only on the sum of η_1 and η_2, which is the measured quantity, and would necessitate beam tube warm up and removal of the H_2. The onset of the isotherm density rise has been observed experimentally in the photodesorption experiments at BINP.[9] If the results shown in Fig. 8 apply to the entire ring, as could occur during initial conditioning, the vacuum limited luminosity lifetime would be degraded below the 150 hrs design goal before reaching one monolayer; ~4.5 hrs for $\bar{v} = 2.1 \times 10^4$ cm / sec and ~40 hrs for $\bar{v} = 1.8 \times 10^5$ cm / sec. The lower of these bounds would require beam tube warm up before reaching one monolayer since, aside from severely limiting luminosity, the power loss by beam gas scattering would approximately equal the synchrotron radiation loss at design intensity and the additional heat load would overload the cryoplant capacity. The primary uncertainty in making projections of gas density in the Collider without a liner is the unknown velocity of the molecules, or equivalently, the absence of a direct measurement of density inside the 4.2 K-beam tube.

5.2 Lower bound Collider luminosity lifetime and scattered beam power due to beam gas interactions in a liner

Beam gas density with a liner is estimated using the H_2 and CO desorption coefficients measured in Fig. 4 and an assumed conductance in Eqn. (8). Again we encounter the

unknown molecular velocities. If the liner were at a temperature high enough not to be cryosorbing then it would be correct to assume the molecules are in thermal equilibrium with the liner.[12] Here we are interested in a liner near the 4.2 K temperature of the magnet cryostat and this is not necessarily a correct assumption. However, if we make this assumption it gives a lower bound on the luminosity lifetime and an upper bound on the scattered beam power due to beam gas interactions and this is useful. For the calculations we have assumed a conductance $C = pN_h A_h \bar{v} / 4$ with 600 2 mm diameter holes per meter, $\bar{v}$ corresponding to 4.2 K and a molecular transmission probability p = 0.6. In actual practice it may be desirable to use short slots rather than circular holes to reduce the beam impedance and increase the safety margin for beam instabilities.[13] However experimentally and theoretically the safety margin seems acceptable even with this number of circular holes.[14] The results are shown in Fig. 9. Except at the earliest times beam gas scattering is dominated by CO. The luminosity lifetime is predicted to reach 150 hrs after conditioning with $\Gamma \sim 10^{22}$ photons/m. The scattered beam power initially reaches only 0.018 W/m, 13% of the synchrotron radiation power, and then decreases monotonically. Clearly this would be acceptable vacuum performance. If the mean molecular velocities are higher than assumed here then the conductance could be reduced.

For the calculations in Fig. 9 we have included only H_2 and CO. An additional consideration that should be examined is the possibility of other heavy molecules besides CO which may be present but were not observed in the photodesorption experiments due to condensation on the 77-K tube connecting the RGA with the 4.2 K-beam tube. Again a direct measurement of gas density inside the beam tube would be useful for this purpose.

6.0 New techniques for measurement of gas density in a 4.2 K beam tube

The 4.2 K photodesorption experiments discussed in Section 4.2 used a room temperature RGA so the actual gas density inside the beam tube is known only up to a scale

factor depending on the ratio of mean molecular speeds at room temperature and inside the beam tube. Since the beam tube is cryosorbing, it is likely that the photodesorbed molecules not yet stuck to the wall have a mean speed greater than molecules in thermal equilibrium with the walls. Some evidence for this can be obtained from analysis of the experiment of Bintinger *et al.*[5] Methods of measuring the gas density directly inside the 4.2 K-beam tube are constrained by the presence of the photon flux and the low temperature environment. Two promising methods are being pursued: (1) charge exchange of H^-/H^+ atomic beams and (2) annihilation of a low energy positron beam. These concepts have been developed to the point where it is conceivable to use them in 4.2 K photodesorption experiments in the next few months. The key ideas will be described in the following two sections.

6.1 The H^-/H^+ ion beam method

The H^-/H^+ ion beam method uses various stripping or charge exchange reactions of H^- or H^+ beams on neutral gas molecules; for example $H^- + H_2 \rightarrow H^0 + H_2 + e$, $H^+ + H_2 \rightarrow H^0 + H_2^+$, $H^- + H_2 \rightarrow H^+ + H_2 + 2e$, $H^+ + H_2 \rightarrow H^- + \ldots$. Fig. 10 shows a diagram of the method for an H^+ beam. A proton beam (~20 keV, ~1 μA) is extracted from an rf ion source, transported to the cryostat and injected along the axis of the beam tube with a bending magnet. Neutral hydrogen atoms produced by interaction with beam gas molecules are separated from H^-/H^+ by another bending magnet at the beam tube exit and detected with a secondary electron multiplier. Two pairs of small superconducting dipole magnets near the center of the beam tube are used to offset a ~20 cm segment of the H^+ beam orbit. The detector is lined up to observe H^0 produced along this offset segment, thus providing a localized measurement of beam gas density. If necessary, background due to synchrotron radiation photons can be discriminated against by gating the detector on between bursts of synchrotron radiation. We can estimate the signal intensity from:

$$R = \varepsilon n \sigma_{10} L I_{H^+} \tag{9}$$

where n is the H_2 gas density ($3 \times 10^8/cm^3$), σ_{10} the cross section for $H^+ + H_2 \rightarrow H^0 + H_2^+$ (~6×10^{-16} cm^2 at 20 keV), L the path length of observation (~20 cm), I_{H^+} the proton current (~1 μA) and ε is the detector efficiency (~1.0). Inserting the numbers in parentheses we get R = 2×10^7 counts/sec. This is a high sensitivity method. It may be possible to observe the decay of the neutral gas density following fast extraction of the VEPP2M electron beam and thus obtain an estimate of the product of sticking coefficient and mean molecular speed.

6.2 The positron method

Figure 11 shows a schematic of the BNL positron method of gas density measurement inside a 4.2 K beam tube photodesorption experiment. Photodesorbing synchrotron radiation photons are incident from the right and are intercepted on the beam tube wall at ~10 mrad. For clarity they are omitted from the diagram. Positrons from a ^{22}Na source on the left (e^+ end point = 0.540 MeV) are moderated with a tungsten foil. Moderation efficiency is ~1–5 × 10^{-4}. The moderated e^+ leaving the foil are accelerated to the peak of the positronium formation cross section ~30 eV and separated from high energy unmoderated e^+ with a pair of E × B filters. The offset path of the E × B filters allows for absorption of the unmoderated high energy e^+ and shields ^{22}Na gamma radiation from the experiment. An electrostatic mirror reflects the positrons from the left, doubling the sensitivity; the second E × B filter deflects returning e^+ onto a beam dump. A fraction of positrons in the beam tube capture an electron from gas molecules in the tube to form positronium; the pair of 0.511 MeV annihilation gammas are detected in coincidence with NaI crystal detectors. A magnetic field B~50–100 G, produced by an axial array of Helmholtz coils, is used to guide the e^+ beam. The signal rate R may be estimated from:

$$R = \varepsilon^2 \left(\frac{2\Omega}{4\pi} \right) n\sigma L I_{e^+} \tag{10}$$

where Ω ($\approx \pi$ steradians) is the smallest solid angle of the two NaI detectors, n ($\approx 3 \times 10^8$ H_2/cm^3) is the gas density, σ ($\approx 4 \times 10^{-16}$ cm^2 for H_2) is the cross section for formation of positronium, L ($\approx$ 14.0 cm) is the length of the interaction region viewed by the detectors, I_{e^+} ($\approx 3 \times 10^5$/sec for a 45 mCi ^{22}Na source) is the number of e^+ per second passing through the interaction region and ε ($\approx$ 0.4) is an overall detector efficiency factor including attenuation of the gamma rays by the walls of the cryostat. If we insert the numbers given in parentheses we obtain ~150 counts/hr, at least an order of magnitude greater than the anticipated random coincidence background. This counting rate will be adequate for the usual photodesorption experiments in which desorption coefficients are measured over periods of days.

7.0 Summary of Issues and Future work

Significant progress has been made understanding photodesorption in a cryosorbing beam tube. We now have a method of measuring photodesorption coefficients of tightly bound and physisorbed H_2 in a 4.2 K-beam tube and data on electrodeposited Cu up to an integrated photon flux ~10^{22} photons/m, the equivalent of ten days of SSC operation. The H_2 desorbed in these experiments corresponded to ~3.4 monolayers and extrapolate to 10–20 monolayers in one year of SSC operation. Since at least one beam tube warm up and pump out is required per monolayer, these results favor a liner approach to the beam tube vacuum system unless an alternate beam tube material or conditioning process can be found which reduces the desorbable H_2 by an order of magnitude. In order to better understand long term behavior it is desirable to extend the range of measurement to one year of operation or ~2×10^{23} photons/m. This would be possible with experiments running about two weeks in high intensity beamlines that have been constructed at the BINP

VEPP2M storage ring and the BNL NSLS VUV ring. In order to make accurate quantitative predictions of proton collider beam tube vacuum it is necessary to know the molecular sticking coefficients and mean molecular speeds. Photoelectron emission spectroscopy is being applied at BNL to measure the build up of gas on a 4–5 K surface at a controlled dosing rate, thus giving estimates of the sticking coefficients. So far this has been applied to H_2 on clean Cu. The H^-/H^+ ion beam and positronium annihilation methods of direct gas density measurement in a 4.2 K-beam tube are at a point where experimental results could be expected in the next few months. Simultaneous measurement of gas density with a room temperature RGA would give an estimate of mean molecular speed. In addition, the H^-/H^+ ion beam method looks like it would have enough sensitivity to measure the decay time of neutral density following fast extraction of the VEPP2M electron beam and this will provide a measurement of the product of mean molecular speed and sticking coefficient. Finally hydrogen depth profiles have been measured with nuclear reaction analysis for some of the beam tube materials used in photodesorption experiments. The results have shown that electrodeposited Cu and high purity bulk Cu have very similar profiles, and both exhibit a ~100 Å surface layer which can account for a sizable fraction of the H_2 desorbed in the photodesorption experiments, which is also nearly the same for these two materials. How much future progress will be made on these activities is now uncertain due to the decision by the United States Congress to discontinue funding the SSCL. It is hoped that termination of the SSCL will allow some additional tasks to be carried out so the information will be available to whatever next generation superconducting proton collider is eventually built.

The Superconducting Super Collider Laboratory is operated by University Research Associates Inc. for the U.S. Department of Energy under Contract No. DE-AC35-89ER40486.

References

[1]SSC Central Design Group, "Conceptual Design of the Superconducting Super Collider," SSC-R-2020. March (1986)

[2]LHC Study Group, "Design Study of the Large Hadron Collider (LHC)," CERN 91-03 (1991).

[3]R. Carcagno, W. Schieller, H.-J. Shih, X. Xu and A. Yucel, *Proceedings of Supercollider IV*, New Orleans (1992)

[4]I.S. Baishev, A.I. Drozhdin and N.V. Mokhov, "Beam Loss and Radiation Effects in the SSC Lattice Elements," SSC-306. November (1990).

[5]D. Bintinger, P. Limon, H. Jostlein and D. Trbjovic, "Status of the SSC Photodesorption Experiment," SSC-102(1986). and D. Bintinger, P. Limon and R. Rosenberg, J. Vac. Sci. Technol. **A8**, 2856 (1990).

[6]C. L. Foerster, C. Lanni, I.L. Maslennikov and W.C. Turner, "Photon Desorption Measurements of Copper and Copper Plated Beam Tubes for the SSCL 20 TeV Proton Collider," This conference.

[7]W.C. Turner, "Dynamic Vacuum in the Beam Tube of the SSCL Collider – Cold Beam Tube and Liner Options," SSCL-Preprint-404 (1993). Proc. of 1993 IEEE Part. Acc. Conf., Washington, D.C., p. 3833 (1993).

[8]S. Brunauer, P. Emmett and E. Teller, J. Chem. Soc. **60**, 309 (1938).

[9]V.V. Anashin, O.B. Malyshev, V.N. Osipov, I.L. Maslennikov and W.C. Turner, "Investigation of Synchrotron Radiation Induced Photodesorption in Cryosorbing Quasi-Closed Geometry," SSCL-Preprint-517 (1993). Accepted for publication in *JVST A*.

[10]S. Anderson, L. Wilzen, M. Persson and J. Harris, Phys. Rev., **B40**, 8146(1989).

[11]W.A. Lanford, Nucl. Instr. and Meth. **B66**, 65 (1992).

[12]W.C. Turner, "Model of a 80K Liner Vacuum System for the 4.2K Cold Bore of the SSCL 20 TeV Proton Collider," SSCL-SR-1224/3 (1993). Submitted for publication.

[13]V. Thiagarajan, T. Barts, S. Kurennoy and W. Chou, "Calculation of the Coupling Impedances of Holes and Slots on the Liner Using Mafia and Scaling," Report in preparation.

[14]E. Ruiz, L. Walling, Y. Goren and N. Spayd, "Beam Coupling Measurements and Simulations of a Beam Pipe Liner with Pumping Holes or Slots," SSCL-Preprint-351 (1993). To appear in Proc. of 1993 IEEE Part. Acc. Conf., Washington, D.C., p. 3405 (1993).

Tables

Table I: Comparison of the 294 K photodesorption yield of hydrogen with the NRA analysis of hydrogen surface density.

Material	Photodesorbed molecular hydrogen (H_2) at $\Gamma = 10^{23}$ photons/m	NRA surface density of protons (H)
Silvex elec. Cu	1.0 Torr l/m H_2 3.3×10^{16} H_2/cm^2	2.3×10^{16} H/cm^2
Hitachi 10100 Cu	0.8 Torr l/m H_2 2.6×10^{16} H_2/cm^2	2.6×10^{16} H/cm^2

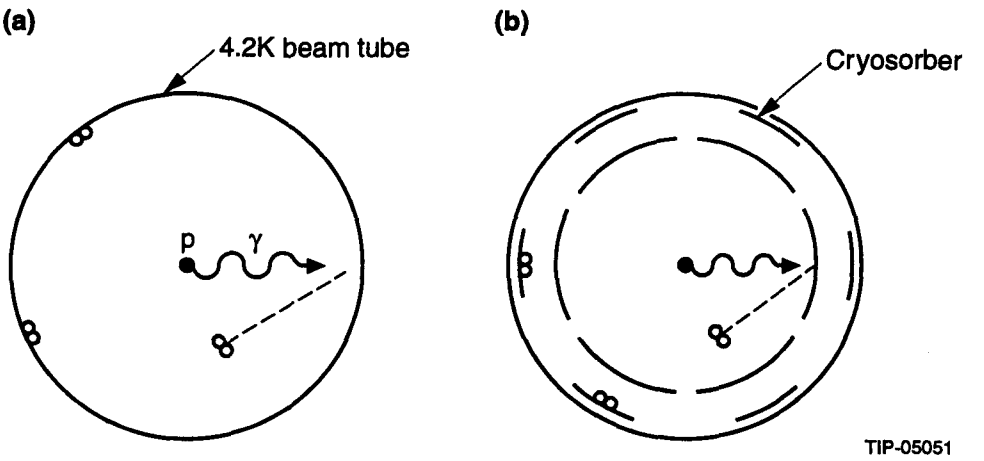

Fig. 1. Schematic of simple beam tube and liner configurations.

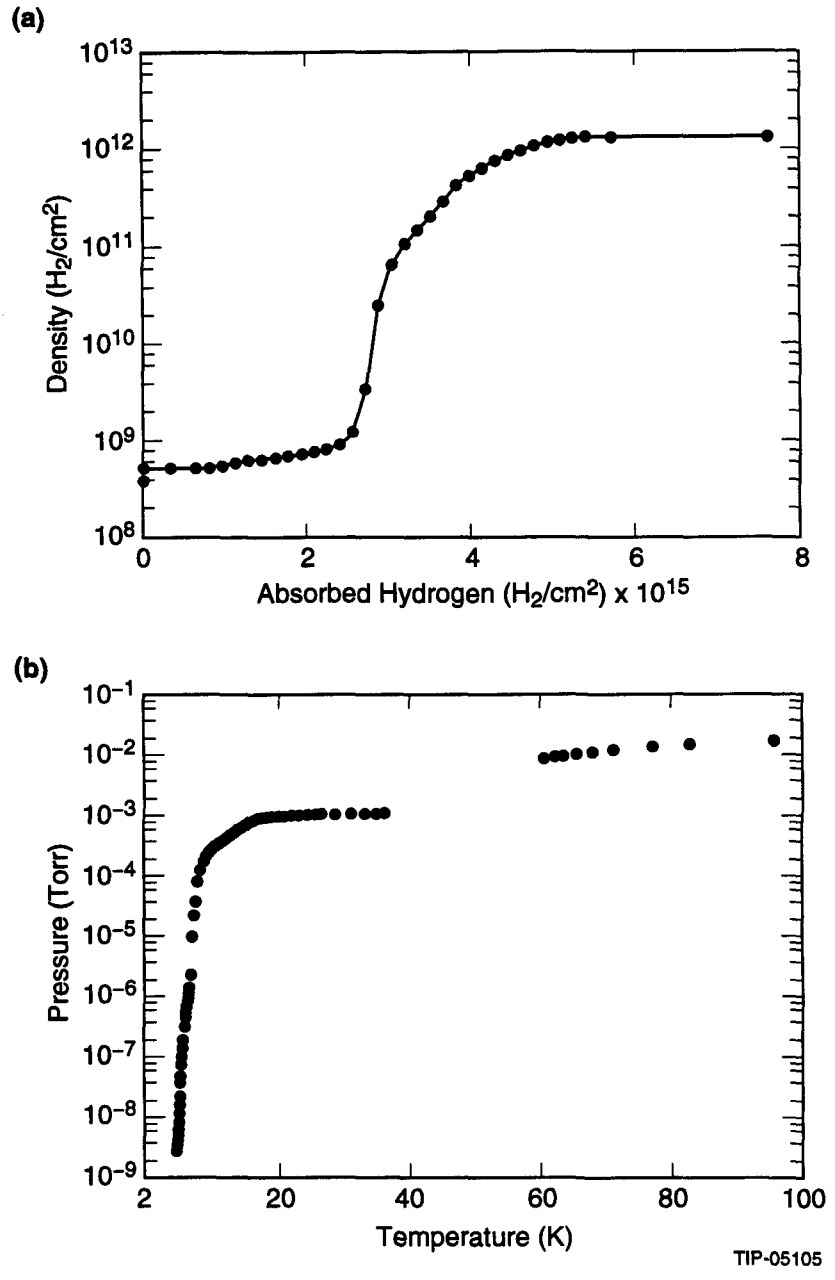

Fig. 2. (a) 4.2 K H_2 isotherm on electroplated Cu, (b) thermal desorption pressure of H_2 and CO versus temperature.

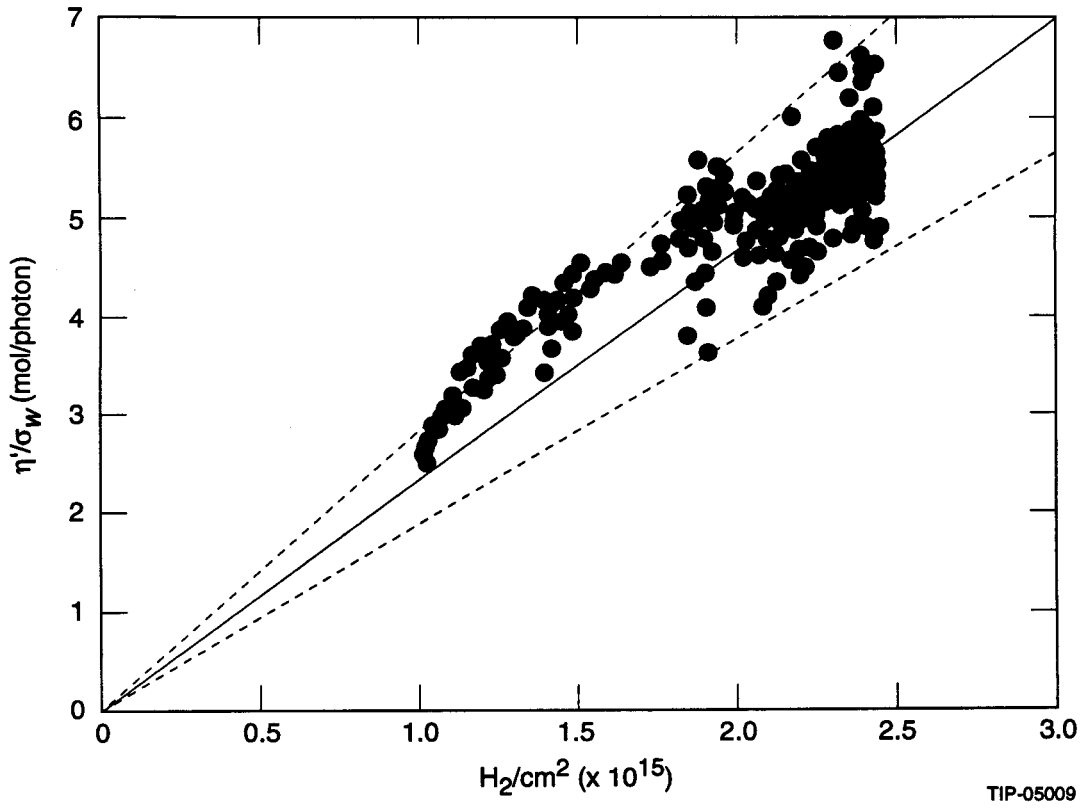

Fig. 3. The photodesorption coefficient η'/σ_w of physisorbed H_2 versus the surface density of adsorbed H_2.

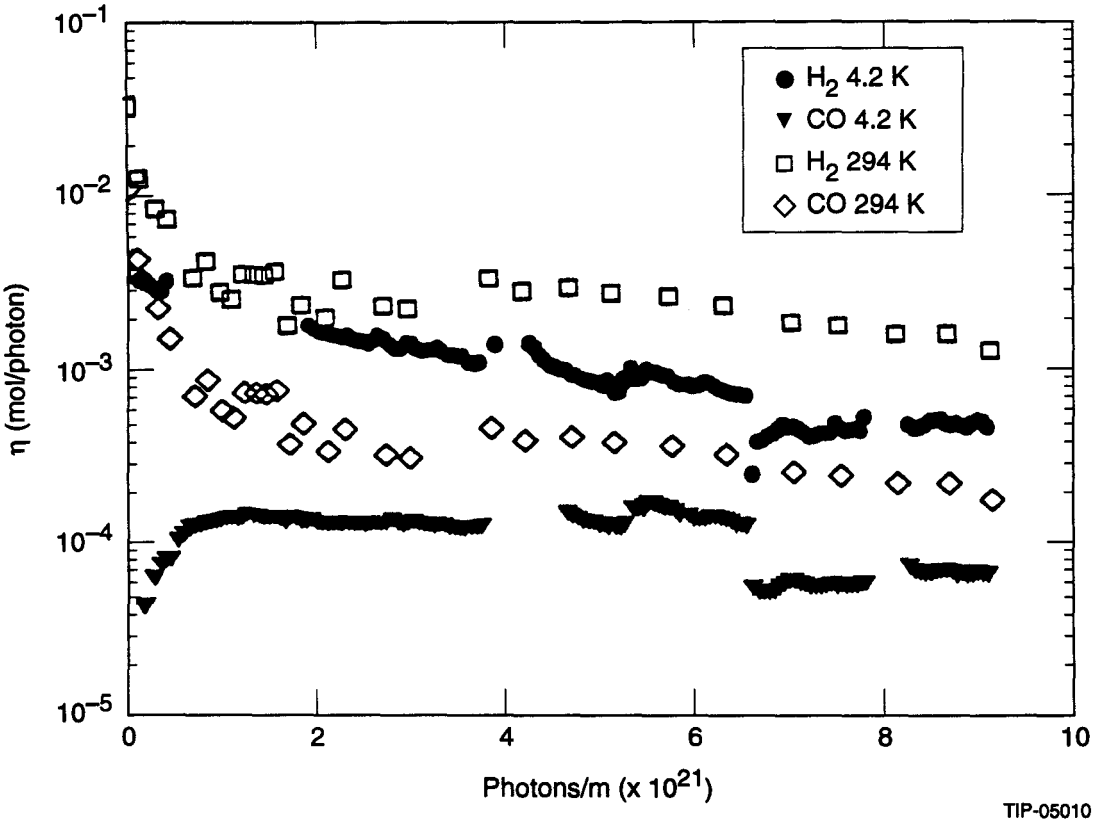

Fig. 4. $\eta(H_2)$ and $\eta(CO)$ versus integrated photon flux for electrodeposited Cu. Data are shown for 4.2 K and 294 K experiments.

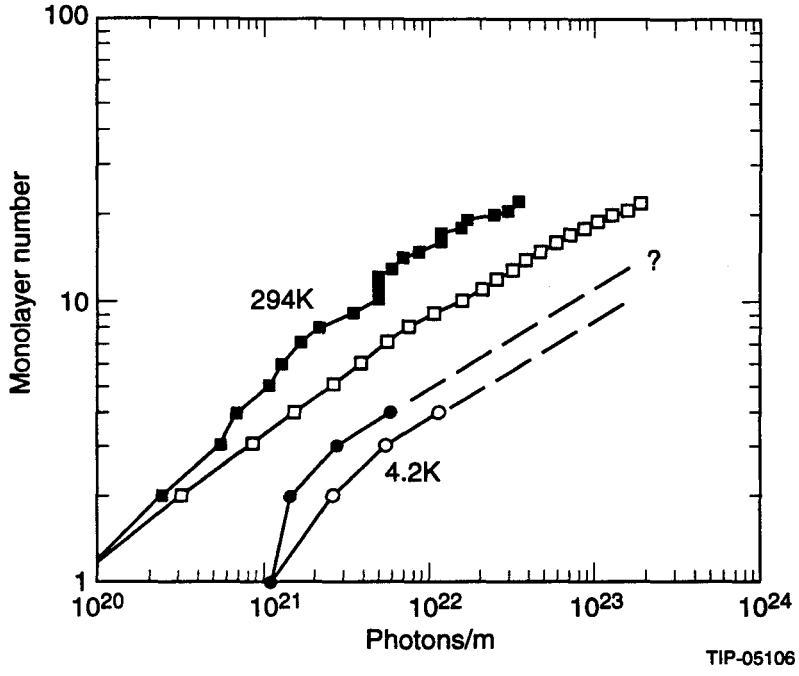

Fig. 5. Number of H_2 monolayers desorbed from electrodeposited Cu versus cumulative (open symbols) and differential (closed symbols) integrated photon flux. Data are shown for 4.2 K and 294 K experiments. The differential data give the integrated photon flux required to desorb each successive monolayer; the cumulative data give the total flux required to desorb N monolayers. One monolayer = 3.0×10^{18} H_2/m.

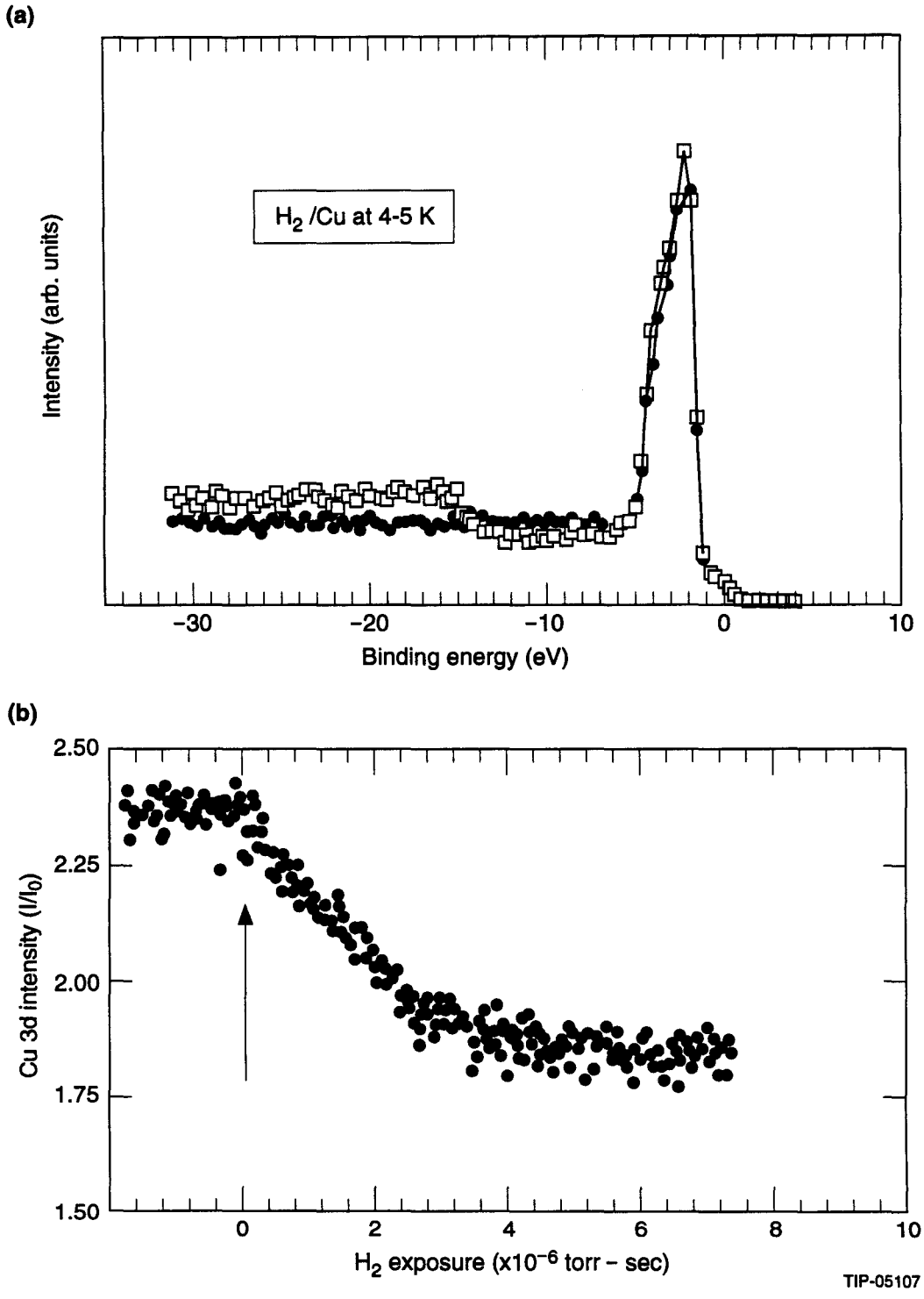

Fig. 6. (a) photoemission electron energy spectra on a 4–5 K clean Cu surface exposed to H_2 dosing, solid circles 0.0 Langmuir, open squares 7.4 Langmuirs, (b) attenuation of the Cu 3d photoelectron intensity versus H_2 dose.

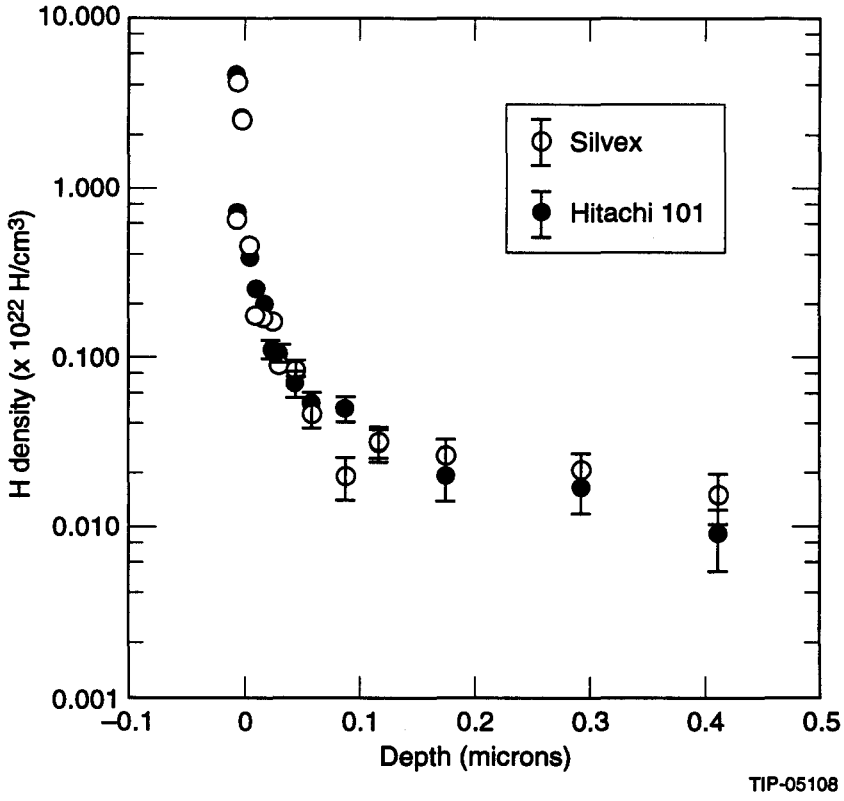

Fig. 7. Depth profile of hydrogen in Silvex electrodeposited Cu and Hitachi 10100 high purity bulk Cu.

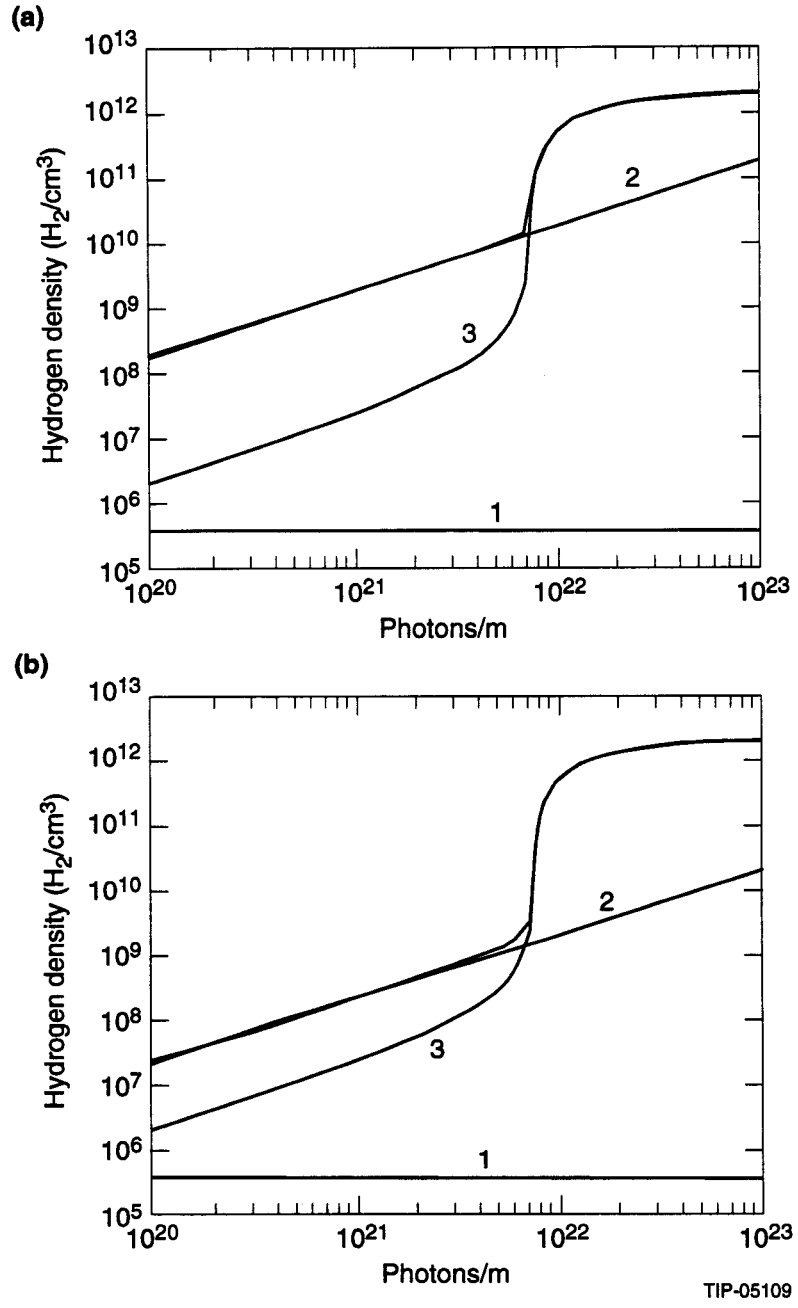

Fig. 8. Model calculations of H_2 density versus photon exposure in a cryosorbing beam tube; (a) $\bar{v} = 2.1 \times 10^4$ cm / sec and (b) $\bar{v} = 1.8 \times 10^5$ cm / sec. The three density components shown are: (1) photodesorption of tightly bound H_2, (2) photodesorption of physisorbed H_2 and (3) the H_2 isotherm.

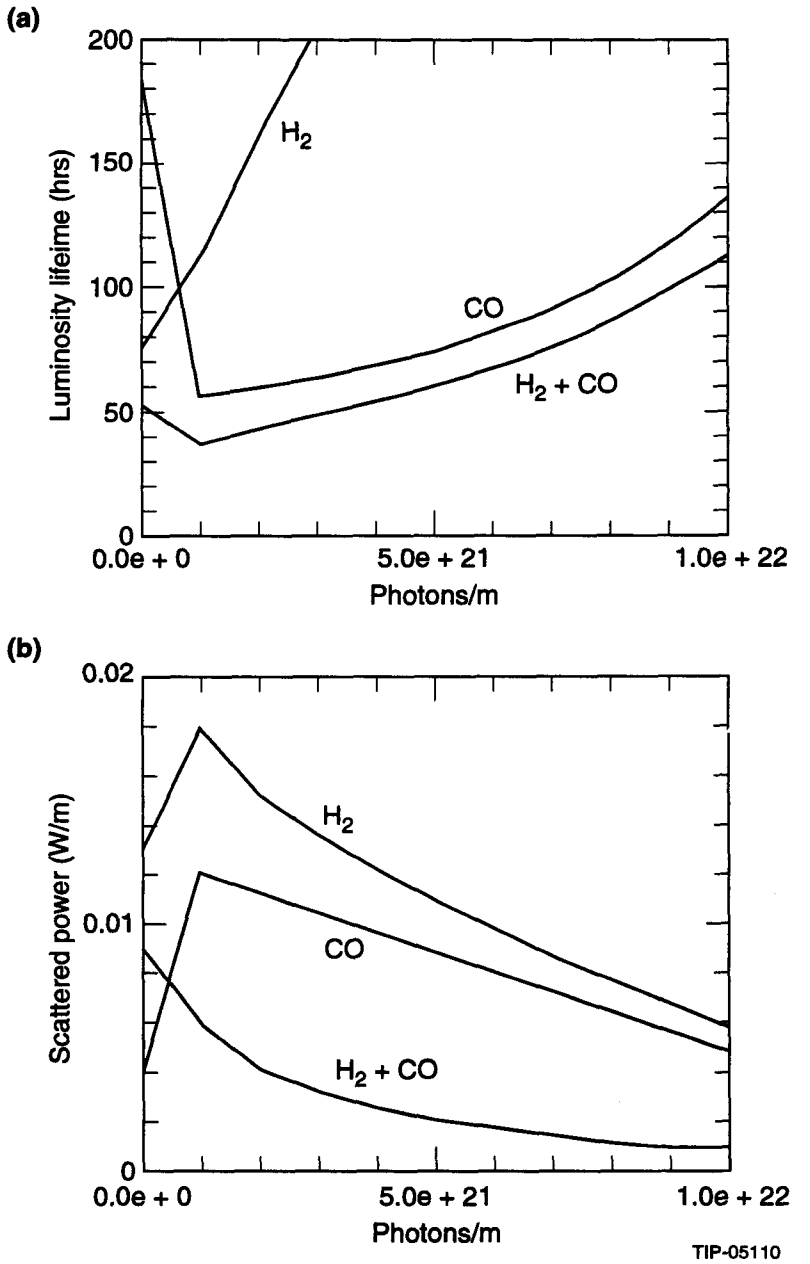

Fig. 9. (a) Lower bound for Collider luminosity lifetime and (b) upper bound for beam power scattered by beam gas interactions versus photon flux for a liner configuration.

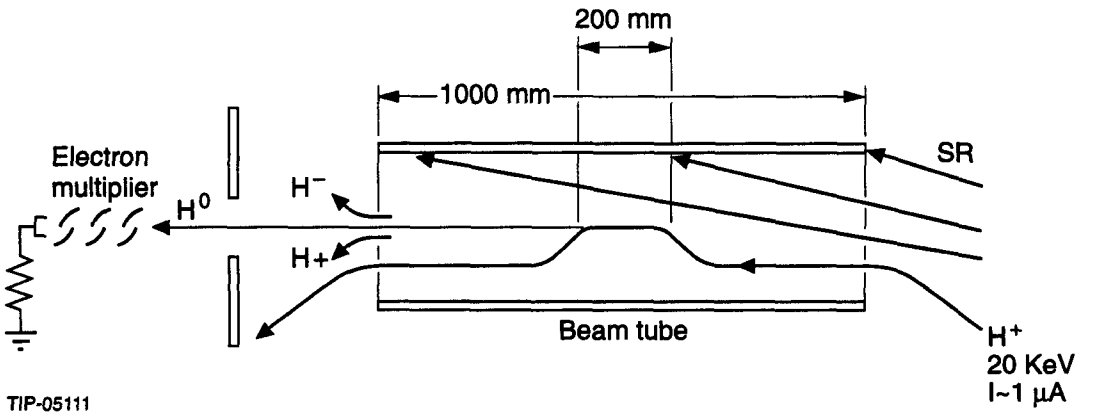

Fig. 10. Schematic of the H^-/H^+ ion beam method of gas density measurement in a 4.2 K-beam tube.

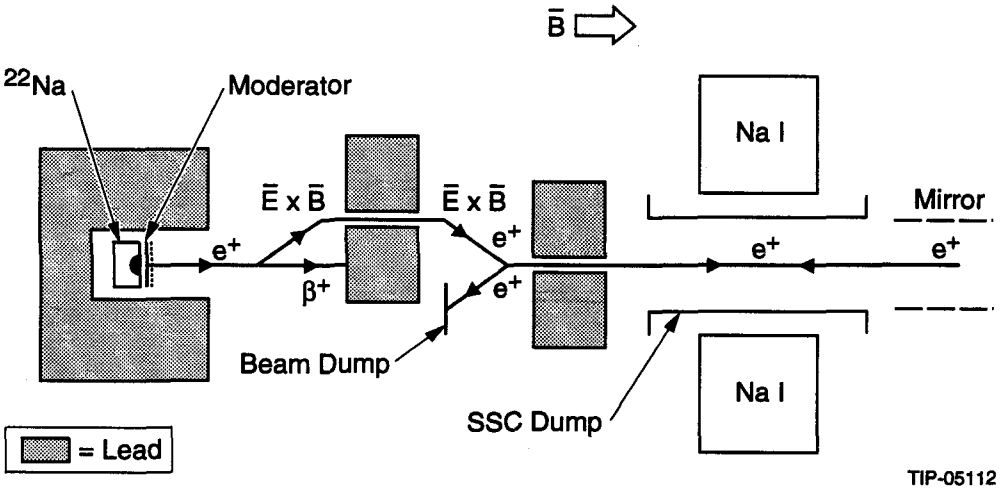

Fig. 11. Schematic of the positron method of gas density measurement in a 4.2 K-beam tube.